Available online at www.sciencedirect.com
SCIENCE DIRECT®
International Journal of Heat and Mass Transfer 47 (2004) 2715–2733
International Journal of HEAT and MASS TRANSFER
www.elsevier.com/locate/ijhmt

Thermal regulation of building-integrated photovoltaics using phase change materials

M.J. Huang [a], P.C. Eames [a,*], B. Norton [b]

[a] *Centre for Sustainable Technologies, School of the Built Environment, University of Ulster, Newtownabbey BT37 0QB, N. Ireland, UK*

[b] *Dublin Institute of Technology, Aungier St., Dublin 2, Ireland*

Received 9 June 2003; received in revised form 1 November 2003

Abstract

Elevated operating temperatures reduce the efficiency of photovoltaic devices. The use of a phase change material to moderate building integrated photovoltaic temperature rise has been investigated by experiments and numerical simulations. Experimental data are used to validate the previously developed two-dimensional finite volume heat transfer model conjugated hydrodynamically to solve the Navier–Stokes and energy equations. A parametric study of a design application is also reported. Temperatures, velocity fields and vortex formation within the system were predicted for a variety of configurations using the experimentally validated numerical model. Temperature distributions predicted for different insolation and ambient temperatures at the photovoltaic surface show that the moderation of temperature achieved can lead to significant improvements in the operational efficiency of photovoltaic facades.

Keywords: Phase change material; Photovoltaics; Thermal control; Building integration

1. Introduction

Only about 16% of the solar energy incident on a photovoltaic (PV) device is converted to electricity; the remaining insolation absorbed is transformed into heat [1]. For crystalline silicon solar cells the associated elevation of PV temperature reduces solar to electrical energy conversion efficiency by 0.4–0.5% K^{-1} [2,3]. Independent testing of the "BP Saturn" PV cell showed a reduction in conversion efficiency from 15.8% at 25 °C to 12% at 80 °C, yielding a temperature coefficient relating conversion efficiency to module temperature of −0.44% K^{-1} [4]. Active heat dissipation in building integrated PV (BIPV) using air or water cooling can require high levels of maintenance. In the most common passive approach, a duct arranged behind the PV module or its mounting system allows natural convection and wind induced air-flow from the back of the PV panel [4,5]. Accrual of airborne dust in inlet grilles and on duct surfaces can ultimately cause a reduced rate of heat transfer from the PV [6,7].

Phase change materials (PCMs) absorb a large amount of energy as latent heat at a constant phase transition temperature and are thus used for passive heat storage and temperature control of electronics [8–11]. Solid–liquid transition PCMs have been incorporated into gypsum wallboards to provide passive energy storage in buildings [12,13]. Experimental and numerical studies into glazings filled with different thicknesses of PCM were presented by Ismail and Henriquez [14]. The thermal performance of solar-aided latent heat storage systems have been theoretically and experimentally studied by Esen [15] and Comakli et al. [16]. A good understanding of the fundamental heat transfer processes involved is essential for accurately predicting the thermal performance of PCM systems and for avoiding costly system over design. There are problems associated with the non-linear motion of the solid–liquid interface,

* Corresponding author.
E-mail address: pc.eames@ulst.ac.uk (P.C. Eames).

0017-9310/$ - see front matter © 2004 Elsevier Ltd. All rights reserved.
doi:10.1016/j.ijheatmasstransfer.2003.11.015

Nomenclature

A	area of the front surface of PV/PCM system (m^2)
C_P	specific heat ($J\,kg^{-1}\,K^{-1}$)
C	specific heat ($J\,kg^{-1}\,K^{-1}$)
g	gravitational constant ($m\,s^{-2}$)
H	latent heat ($J\,kg^{-1}$)
h_c	heat transfer coefficient ($W\,m^{-2}\,K^{-1}$)
I_T	insolation on photovoltaic ($W\,m^{-2}$)
k	thermal conductivity ($W\,m^{-1}\,K^{-1}$)
m	mass (kg)
P	pressure (Pa)
Q_S	sensible heat ($J\,kg^{-1}$)
Q_L	latent heat in phase change material ($J\,kg^{-1}$)
S	general source term (J)
T	temperature (°C)
T_{amb}	ambient temperature (°C)
T_m	melt temperature (°C)
$T_{PV,t}$	temperature on PV at time t (°C)
$T_{PV,t+\Delta t}$	temperature on PV at time $t+\Delta t$ (°C)
t	time (s)
Δt	time step (s)
u, v	velocities ($m\,s^{-1}$)
Δx	depth of the PV/PCM system (m)
ρ	density ($kg\,m^{-3}$)
μ	viscosity ($m^2\,s^{-1}$)

Subscripts

L	liquid phase
S	solid phase

the presence of buoyancy driven flows in the melt, the volume expansion of the PCM and the density change in the PCM that takes place upon melting/solidification [17].

Reviews of the general numerical techniques for the solution of solid–liquid phase change problems have been undertaken by Dincer and Rosen [17] and Voller [18]. For the conduction-dominated phase, in some models the effects of natural convection in the melt phase is incorporated in the model by using an enhanced thermal conductivity (or thermal diffusivity) for the melt [19–23]. Studies have been undertaken that focus on the melt process inside containers using two-dimensional numerical models for rectangular cross section containers [24–27] and for cylindrical containers [28–30]. In spite of the impressive number of articles published on the subject over the last 15 years, simulation of PCMs for real thermal applications with cyclic melting and solidification subject to realistic boundary conditions remains a challenging task [17].

Incorporating a solid–liquid PCM with a phase change similar to the PV characterising temperature of 25 °C for the thermal regulation of building integrated PV under cyclic time-dependent solar energy input is a novel approach to BIPV temperature control. Depending on ambient conditions, a PV/PCM system may enable the PV to operate near its characterising temperature and thus with good solar to electrical conversion efficiency. An additional potential benefit is that the energy stored in the PCM may be released to provide building heating at night. An extensive experimental test campaign has been undertaken on the thermal behaviour of a phase change material, when used to moderate the temperature rise of PV in a PV/PCM system [31,32]. A transient numerical model for predicting the thermal and fluid-dynamic behaviour has been developed [31,32] to optimise the PV/PCM system design. This paper describes the experimental validation and application of the developed PV/PCM simulation model. This is the first time a model for a PV/PCM system has been validated using experimental data, with a comparison of measured isotherms to those predicted, with photographs illustrating the melt process. Using the validated numerical model, behaviour is predicted for a range of PV/PCM systems and conditions.

2. Thermal transfer in the PV/PCM system

Heat transfer external to the PV/PCM system is presented in Fig. 1. The incident energy I_T absorbed by

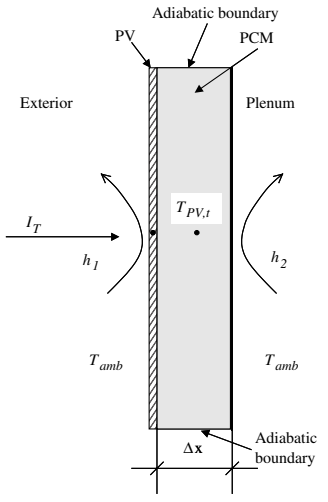

Fig. 1. Schematic diagram of heat transfer in PV/PCM system.

the PV and transformed into heat can be transferred to the PCM in the PV/PCM system. Assuming (i) the initial temperature of the PV T_{PV} is the same as that of the PCM, (ii) the heat transfer coefficients from the front and rear surfaces have the fixed values h_1 and h_2, (iii) that in time Δt the temperature change within the PCM is from $T_{PV,t}$ to $T_{PV,t+\Delta t}$ and (iv) there is no heat lost from the top and bottom adiabatic boundaries of the system. The energy balance for a system when the calculated temperature $T_{PV,t+\Delta t}$ is smaller than the PCM melt temperature T_m is

$$AI_T\Delta t = A(h_1+h_2)(T_{PV,t}-T_{amb})\Delta t + (T_{PV,t+\Delta t}-T_{PV,t})\rho c_P \Delta x A \quad (1)$$

where, A is the surface area, T_{amb} is the ambient temperature. When the calculated temperature $T_{PV,t+\Delta t}$ is greater than T_m, thermal energy is used for phase change and the temperature in the PCM remains constant at T_m until the phase change is completed, i.e. the absorbed energy in the PCM is larger than the latent heat of fusion H. The total time for phase change is $\sum \Delta t$ for which this condition holds. The energy balance for the phase transition is

$$\text{i.e. } AI_T\sum \Delta t = A(h_1+h_2)(T_m-T_{amb})\sum \Delta t + H\Delta x A \quad (2)$$

From the incident thermal energy and PCM properties, the volume of PCM ΔxA required to control the temperature of the PV (i.e. the phase transition temperature) may be calculated and the energy stored in the PCM determined by Eq. (2).

A two-dimensional temperature-based finite volume based conjugated heat transfer numerical simulation model, has been developed to predict the thermal behaviour of a PV/PCM system. The non-linear transient model uses Boussinesq's approximation and allows convection and diffusion to be simulated. A fully implicit formulation is used. The developed model can be used to predict the transient temperature distribution and fluid flow field within a two-dimensional region in the PV/PCM system for different insolation, ambient temperatures, convective and radiative heat transfer boundary conditions [32,33].

The governing equations used for PV/PCM system [34] with the incorporation of the continuity equation in a Cartesian co-ordinate system are

The momentum equations: (Navier–Stokes equations)

$$\rho\frac{\partial u}{\partial t}+\rho u\frac{\partial u}{\partial x}+\rho v\frac{\partial u}{\partial y}=\nabla(\mu\nabla u)-\frac{\partial P}{\partial x}+\beta(T-T_m) \quad (3)$$

$$\rho\frac{\partial v}{\partial t}+\rho u\frac{\partial v}{\partial x}+\rho v\frac{\partial v}{\partial y}=\nabla(\mu\nabla v)-\frac{\partial P}{\partial x}-\rho g \quad (4)$$

with $\mu=\mu_S=\infty$, $\rho=\rho_S$ in solid regions of the PCM, and $\mu=\mu_L$, $\rho=\rho_L$ in liquid regions of the PCM.

The thermal expansion coefficient, β, is introduced into the v-momentum equation to include the buoyancy force term, according to the Boussinesq's approximation:

$$\rho=\rho_0[1-\beta(T-T_m)] \quad (5)$$

where ρ_0 is the reference density and T_m is the melting or freezing temperature.

Substituting ρ into the last term in Eq. (4) yields

$$-\rho g=\rho_0 g[\beta(T-T_m)-1] \quad (6)$$

The energy equation:

$$\rho\frac{\partial T}{\partial t}+\frac{\partial}{\partial x}\left(\rho uT-k\frac{\partial T}{\partial x}\right)+\frac{\partial}{\partial y}\left(\rho vT-k\frac{\partial T}{\partial y}\right)=S \quad (7)$$

The phase change occurs at a set temperature. In the case of constant specific heat capacities for each phase, the temperature field can be defined as

$$T=\begin{cases} E/c_S & T<T_m \text{ (solid phase)} \\ T_m & 0<E<H,\ T>T_m \text{ (melt zone)} \\ T_m+(E-H)/c_L & E\geqslant H,\ T>T_m \text{ (liquid phase)} \end{cases} \quad (8)$$

The numerical scheme adopted to solve the pressure and velocity was based on a line-by-line reduced bandwidth direct solver.

3. Experiments

A series of experiments were undertaken to study the thermal behaviour of PV/PCM systems [31,32,35]. Three different system configurations were studied:

- Single flat aluminium plate system.
- PV/PCM system without internal fins.
- PV/PCM system with internal fins.

Temperature measurements for a 0.300 m wide by 0.132 m high by 0.0045 m thick aluminium plate covered by selective solar absorbing film (which provides known radiative properties [36]) provided an experimental comparison with predictions for a natural convectively cooled system. The two experimental PV/PCM systems, with and without metal fins provided results which enabled detailed comparison of PV/PCM behaviour with prediction. Both PV/PCM systems had the same external dimensions. As shown in Fig. 2, the front and rear walls of the PV/PCM system and the two fins fixed to the front wall of the system were fabricated from 0.0045 mm thick aluminium plate. The inside dimensions of the container were 0.040 m wide by 0.132 m high by 0.300 m long. The two 0.030 m wide fins extended the full length of the system. The upper and lower horizontal faces and the vertical end faces of the PCM container were made

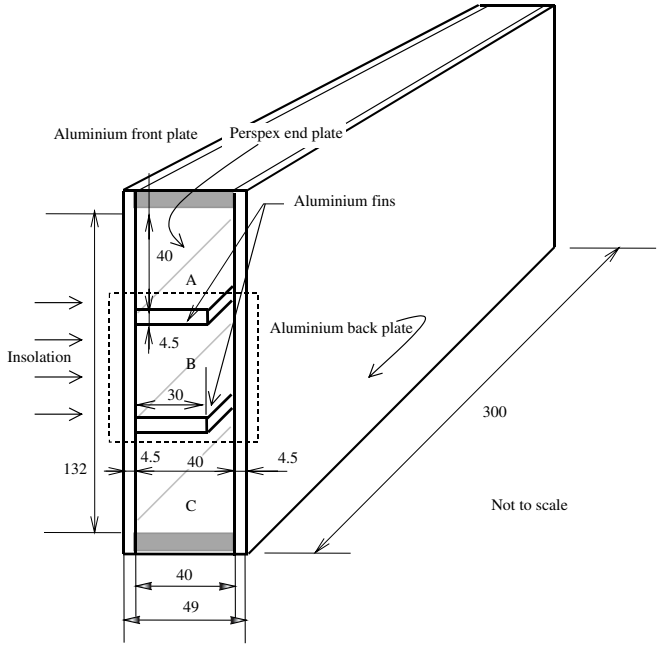

Fig. 2. Schematic diagram of the experimental PV/PCM system with internal fins (dimensions in mm).

of 0.008 m thick clear perspex, insulated with 0.050 m thick polystyrene foam with a thermal conductivity 0.027 $W m^{-1} K^{-1}$. To observe the phase change process the insulation on the vertical end side faces could be removed. The thermophysical properties of the phase change materials and aluminium applicable to experiments and simulations are shown in Table 1. The data sheet provided by the manufacturer "RUBITHERM" indicates the PCMs used in the experiments have stable performance throughout repeated phase change cycles. From the experimental observations there was no deterioration of the PCMs.

The temperatures on the convectively cooled aluminium plate and on the front surface of the PV/PCM system without fins were measured by five T-type copper/constantan thermocouples. For the PV/PCM system with fins, a total of 51 fine 0.2×10^{-3} m diameter wire T-type copper/constantan thermocouples were used to measure the temperatures within the PCM, the temperature of the external surfaces of the PV/PCM system and the ambient temperature with an accuracy of ±0.1 °C. To avoid the inclusion of edge effects, the middle section B of the test system as shown in Fig. 2 was used to study the behaviour of the PCM within the PV/PCM system.

Table 1
Thermophysical properties of "RT25" [37], paraffin wax [38] and aluminium [39]

Property	Phase change material "RT25" (for experiment and validation simulations)	Paraffin wax (for simulation)	Aluminium (for experiment and validation simulations)
Density			
Solid, $kg m^{-3}$	785	830	2675
Liquid, $kg m^{-3}$	749	830	Not applicable
Specific heat capacity			
Solid, $J m^{-3} K^{-1}$	1,413,000	1,593,600	2,415,525
Liquid, $J m^{-3} K^{-1}$	1,797,600	2,705,800	Not applicable
Thermal conductivity			
Solid, $W m^{-1} K^{-1}$	0.19	0.514	211
Liquid, $W m^{-1} K^{-1}$	0.18	0.224	Not applicable
Melting temperature, °C	26.6	32	Not applicable
Latent heat of fusion, $J kg^{-1}$	232,000	251,000	Not applicable

Table 2
Thermocouples locations (label in Fig. 3)

Label	Location	
1–7	4 mm from front plate	Inside PCM
8–14	12 mm from front plate	Inside PCM
15–21	20 mm from front plate	Inside PCM
22–30	28 mm from front plate	Inside PCM
31–39	36 mm from front plate	Inside PCM
40–44	On the centre vertical line	Rear plate
45–49	On the centre vertical line	Front plate
50,51	In air, shielded from radiation sources	Ambient

Table 2 lists the thermocouple locations in the system. Ten thermocouples were positioned equally on the front and back surfaces to measure surface temperatures. Thirty-nine thermocouples as shown in Fig. 3 were located at five identical depths within the PCM to measure the spatial temperature variation. The thermocouple locations along the long axis of the test system were staggered to minimise flow resistance of the thermocouple wires and thus reduce the influence of the presence of the thermocouple wires on the observed behaviour. The measured temperature data from the five sets of thermocouples and those on the surfaces of the system were combined together to produce isothermal contours for a cross-section of section B of the PV/PCM system. The insolation in the experiments produced by a compact MSR 1200HR, 1000 W metal halide lamp was measured using a Kipp & Zonen CM11 pyranometer. The maximum hourly and total radiation measurement errors were 3% and 2% respectively [40]. More detailed descriptions of the measurements process are provided in Huang et al. [31] and Huang [32].

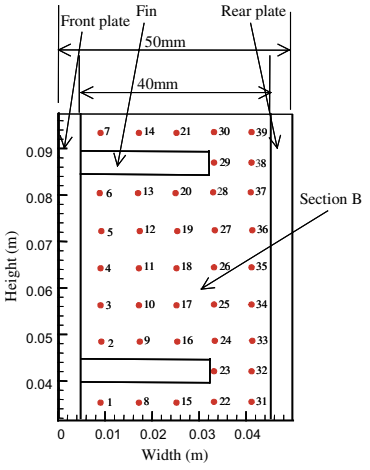

Fig. 3. Distribution of thermocouples within experimental system.

4. Validation

Model validation was performed by direct comparison of predicted temperature values with experimental measurements for which the system geometry, material characteristics and boundary conditions matched as closely as possible. The validation proceeded as follows:

- Validation using a single flat aluminium plate

The insolation intensity was 750 $W m^{-2}$ and the ambient temperature varied by less than 1 °C during the experiment. As indicated in Fig. 4 after 60 min, steady-state conditions were reached. Measured average temperatures on the convectively cooled aluminium plate covered by a selective surface were compared with simulation results as presented in Fig. 4. For the simulation the estimated heat transfer coefficients from both front and rear aluminium plate surfaces were 7.68 $W m^{-2} K^{-1}$. Agreement to within ±0.9 °C between the simulation and experimental results can be seen in Fig. 4. The simulated behaviour of the base case aluminium plate is in good agreement with the respective measured values.

- Validation of the PV/PCM model for a system with no fins in the PCM

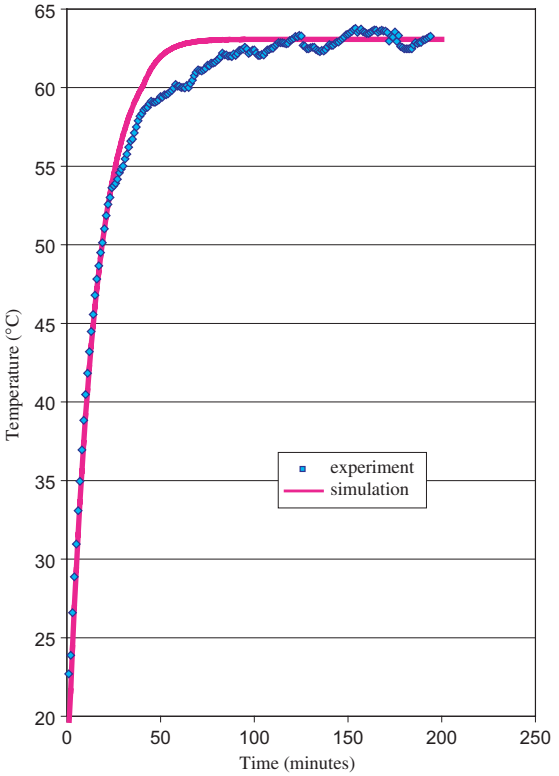

Fig. 4. The predicted and measured temperature at the front surface of the aluminium plate.

For the PV/PCM system without fins the heat transfer coefficients on the front and rear surfaces were assumed to be 12.5 and 7.5 $W m^{-2} K^{-1}$ respectively and the insolation was 750 $W m^{-2}$. The comparison of the measured and predicted temperatures at the front surface of the system with time is presented in Fig. 5. The average difference between predicted and experimental results was ±0.9 °C, with a maximum difference of less than 2 °C. Agreement between predictions and experimental measurements was good.

- Validation of the PV/PCM model for a system with two fins in the PCM

The performance of a PV/PCM system with two fins has been simulated and characterised experimentally. The heat transfer coefficients on the front and rear surfaces were 12.5 and 7.5 $W m^{-2} K^{-1}$ respectively and the insolation was 750 $W m^{-2}$. Simulations used the boundary and applied conditions prevailing experimentally. The Rayleigh number (*Ra*) describes the importance of buoyancy forces which drive convection compared to the diffusive processes (heat and momentum) which act to stabilise convection. The Rayleigh number is given by [41]:

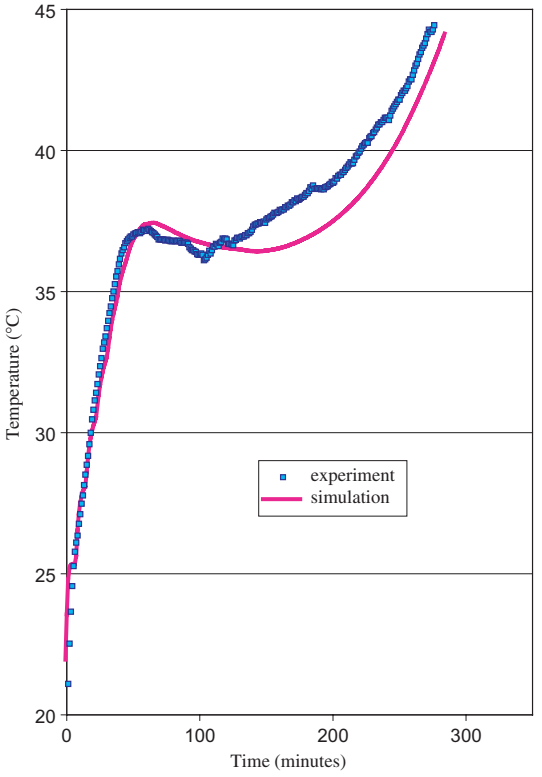

Fig. 5. Average measured and predicted temperature at the front surface of PV/PCM system without fins.

$$Ra \equiv \frac{g\beta \Delta T d^3}{\nu \frac{K}{\rho C_P}}; \tag{9}$$

Using the values for the parameters in the experiments the calculated Rayleigh number *Ra* in the two fined PV/PCM system with a PCM depth of 40 mm was between 1.0×10^4 and 3.0×10^7. From the Rayleigh number it can be concluded that for this system the fluid flow in the PCM container was laminar. Fig. 6 contrasts photographs taken during an experiment with predicted isotherms and predicted velocity vectors during the PCM melt process in the full sized PV/PCM system. The observed and predicted melting trends over the experimental period are in agreement. Enlarged detailed photographs together with measured and predicted isotherms are presented in Fig. 7 for elapsed times of 50 and 100 min. The photographs and predictions of the PCM melt interface locations are in reasonable agreement. To give a detailed temperature comparison, the predicted and experimentally measured average temperatures at the front and rear surfaces of the system and inside the PCM on the horizontal middle line of the PV/PCM system are compared in Fig. 8. The simulation results are found to be in very good agreement with experiment, except for time delay discrepancies. There are two reasons for this: (i) bubbles at the start of melting inhibit heat transfer from the front surface to the PCM, and (ii) the thermocouple holders increased heat transfer to the rear plate and the solid PCM giving measured temperatures inside the PCM lower than the predicted temperatures. However as the outer diameter of the thermocouple holder was 0.15% of the height of the middle section of the system, the increased thermal conductivity resulting from this was 0.07% in the vertical direction and 0.03% in the horizontal direction, there is thus no significant difference between measured and predicted front surface temperatures due to this factor.

5. Parametric analysis

5.1. System types simulated

Using the validated two-dimensional thermofluid finite volume numerical simulation model, PV/PCM systems as specified in Table 3 and Fig. 9 were investigated theoretically. The thermophysical properties of PCM and aluminium fins are listed in Table 1. The simulation model deals with both transient and non-linear effects resulting from the moving interface between the solid and liquid boundary within the melting PCM. Predictions of temperatures and velocities within several PV/PCM systems with and without fins are compared and presented.

In all PV/PCM system types, as shown in Fig. 10, the PV cell is assumed to be attached directly to the alu-

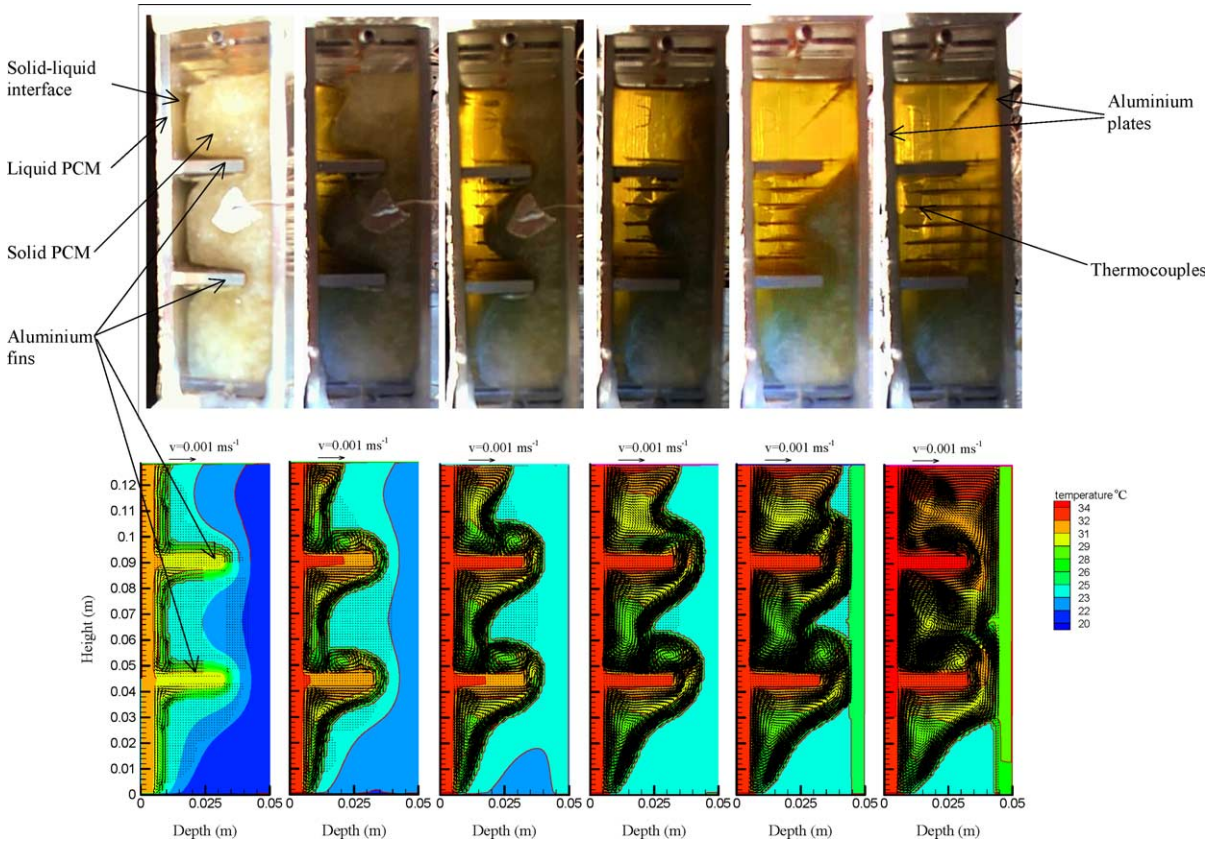

Fig. 6. Photovoltaic image and predicted isotherms and velocities for a PV/PCM system with fins during the PCM melt process.

minium front plate. In the simulations temperatures within the PV/PCM system and that of the ambient environment were all initially set to 20 °C, the heat transfer coefficients from the front and back surfaces of the PV/PCM system were set at 10 and 5 $W m^{-2} K^{-1}$ (to simulate natural ventilation conditions) and the top and bottom boundaries of the system were assumed to be adiabatic. Insolation was kept at a constant value of 1000 $W m^{-2}$. A grid of 1 mm square finite volumes and a variable time step with a minimum value of 0.005 s were used for all simulations.

5.2. The thermophysical performance of PCM in PV/PCM system type I

Fig. 11 presents predicted isotherms and velocity vector diagrams for system type I with a PCM depth of 20 mm at 80, 100 and 118 min respectively. Insolation absorbed on the front surface of the PV/PCM system and conducted through the aluminium plate, increased the temperature of the PCM adjacent to the front aluminium plate causing a thin melt layer in the PCM. As time elapses, the melt front extends into the PCM. The predicted flow is upward, adjacent to the front aluminium plate of the PV/PCM system where the heat input occurs, and downward at the melt–solid interface, where heat is being transferred to the solid and the melt fluid cooled. The PCM in the top of the system melts faster due to convection than that at its base. It can be seen from Fig. 11 that after 118 min all of the PCM has melted and a flow pattern has been established throughout the liquid.

Predictions of temperature in system type I with depth at five different heights at times of 80, 100 and 118 min are presented in Fig. 12. Temperatures on the front surface of the PV/PCM system with the height (39 mm) are the same as within the front aluminium plate due to the high thermal conductivity of aluminium. Heat conduction resistance of the PV panel with aluminium plate can be neglected and the temperature on the PV panel can thus be represented by the temperature on the front surface of the PCM container. A rapid change in the temperature in the PCM adjacent to both the front aluminium plate of the container and at the melt–solid interface can be observed. Due to convection and phase change, the predicted temperature distributions within

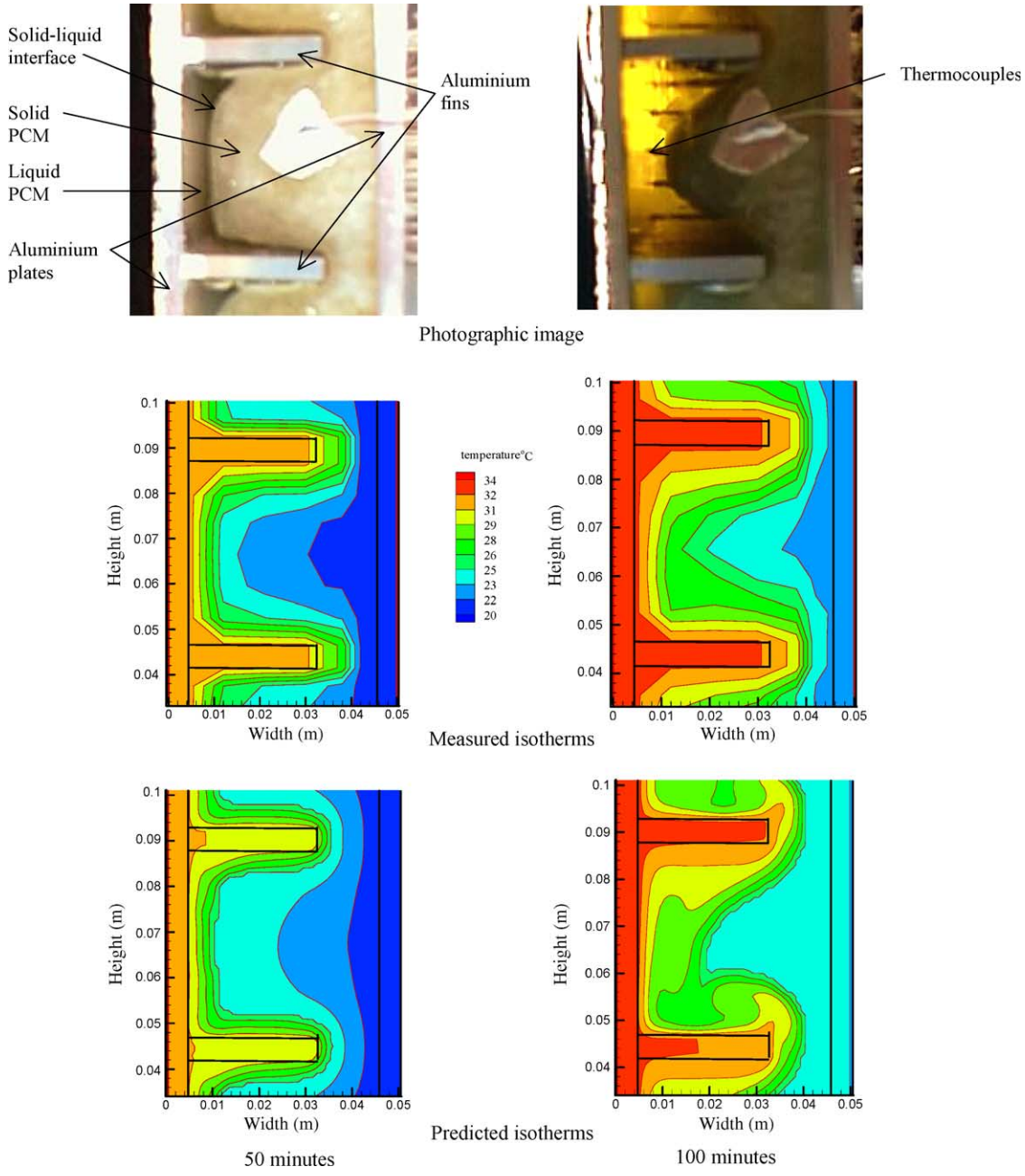

Fig. 7. Photovoltaic image of melt front and measured and predicted isotherms for a PV/PCM system with fins after 50 and 100 min with an average insolation intensity at the front surface of 750 $W\,m^{-2}$.

the PCM container are thermally stratified in the molten PCM with little horizontal variation at each height of the container with elapsed time. The difference of temperature between the base and top of the PCM (39 mm) remains consistent for up to 100 min. After 100 min, as shown in Fig. 12, the convective flow is incident on the rear plate of the container, the temperature of the rear plate rises and there is a resultant increase in the heat transfer rate to the PCM from the rear aluminium wall and the temperature within the PV /PCM system begins to rise quickly. It can be seen from Fig. 12 that after 118 min, the phase change is complete and the temperature of the PCM has increased significantly above the phase change temperature.

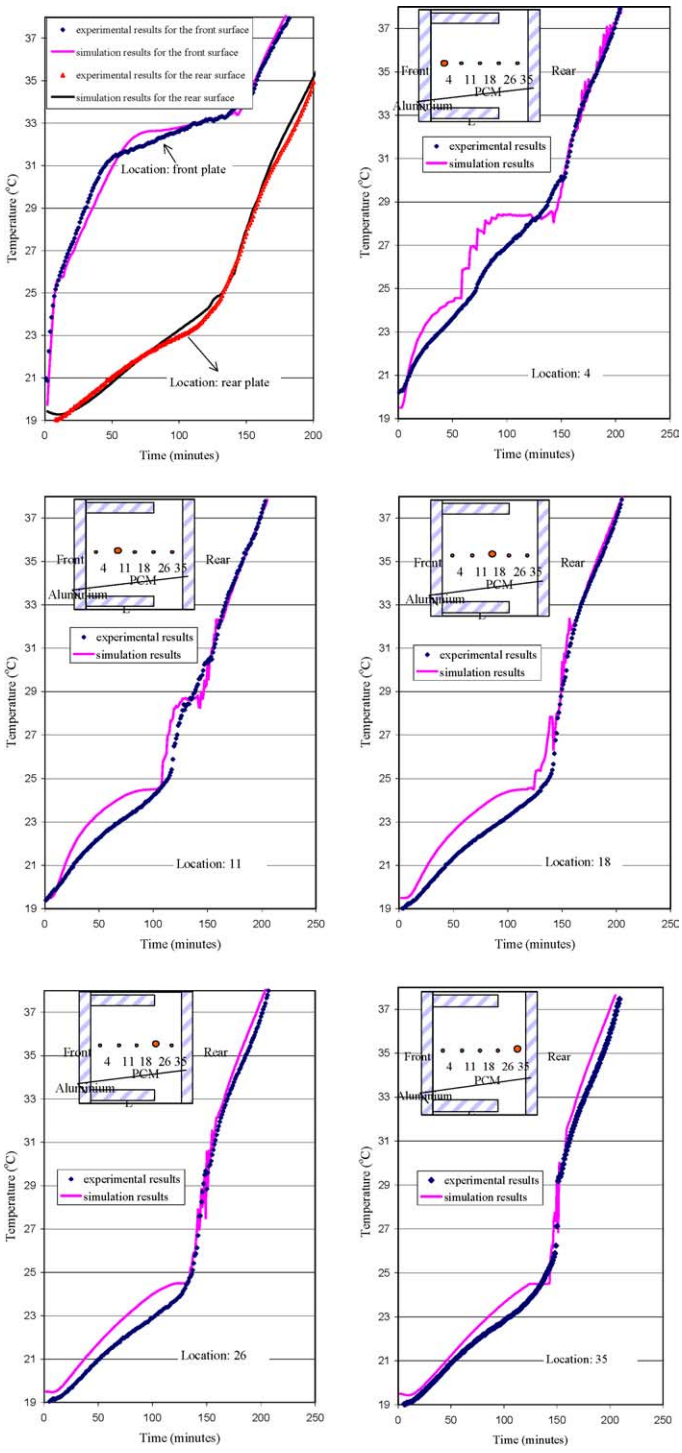

Fig. 8. The predicted and experimentally measured temperatures at the front and rear surfaces of the system and inside the PCM on the horizontal middle line of the PV/PCM system.

Fig. 13 shows the vertical component of velocity within the PCM at different heights after 80 min. Vertical velocity components are large adjacent to the front plate of PV/PCM system and at the melt front. The

Table 3
Specification of PV/PCM systems

System types	Height h (mm)	Depth D (mm)	Number of fins	Fin width x (mm)	Fin length L (mm)
I	40	20,30,50	0	0	0
II	132	20	0	0	0
III	132	20	2,5	2,3,4	15

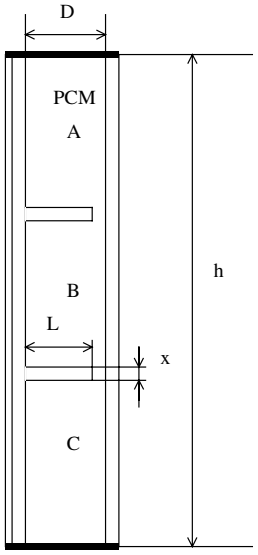

Fig. 9. Geometry of the simulated PV/PCM system.

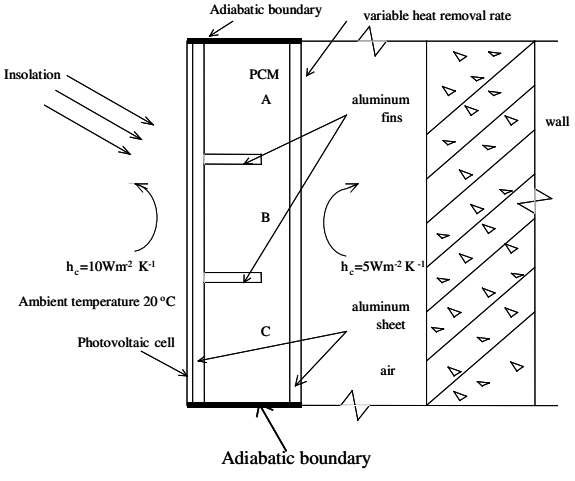

Fig. 10. The structure and boundary conditions of the simulated PV/PCM system type III.

largest vertical velocity component in the PCM either for the up flow or down flow is at the middle height within PV/PCM system type I. The summation of the predicted vertical volume flow rate in the upflow is the

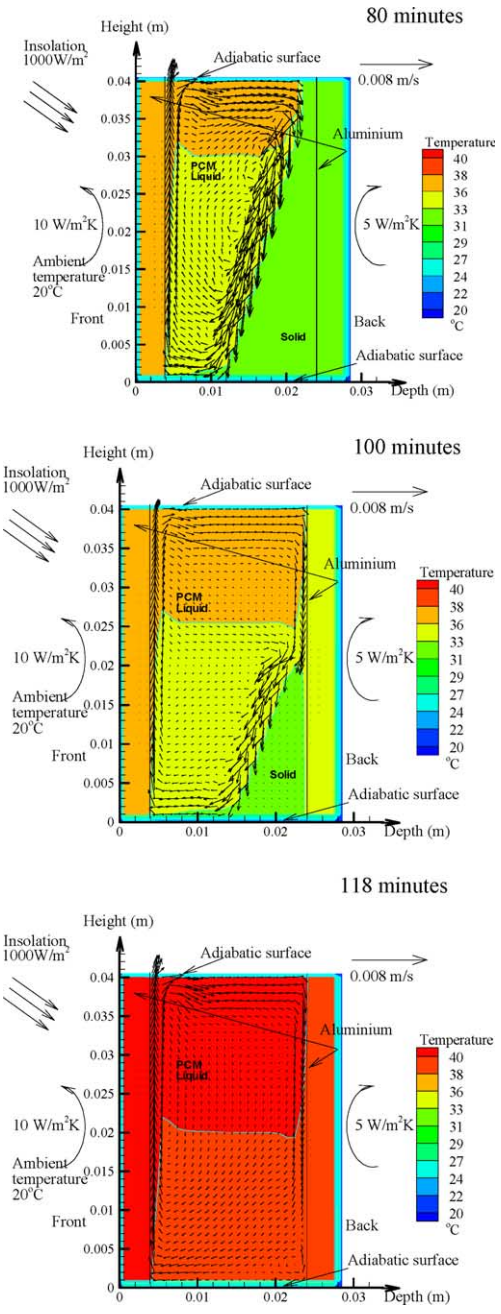

Fig. 11. Predicted isotherms and velocity vectors for system I at 80, 100 and 118 min.

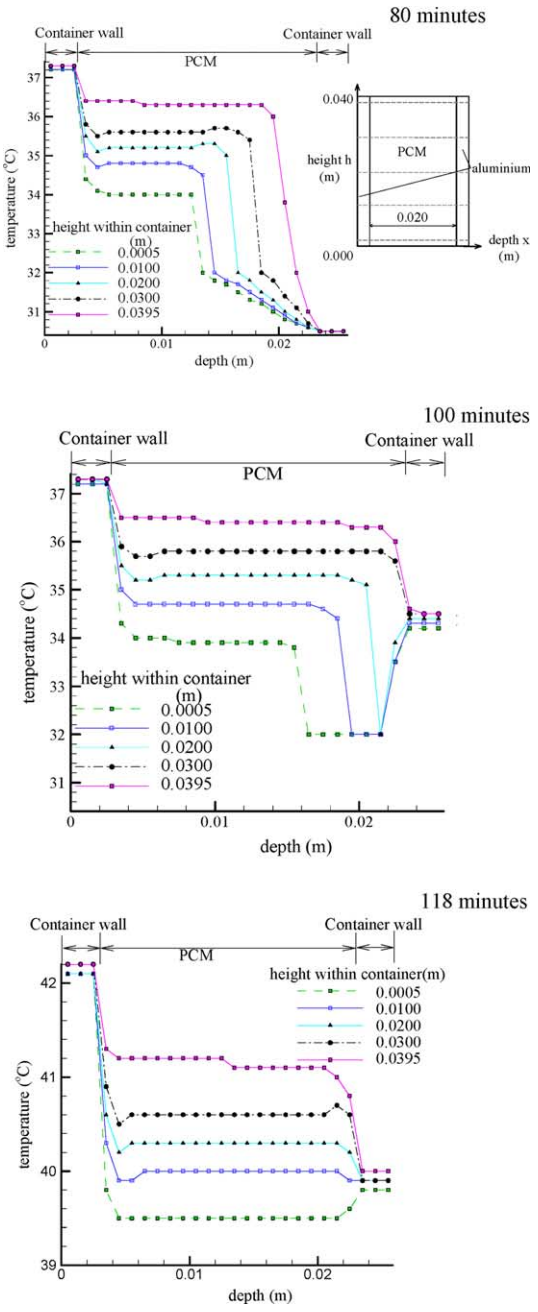

Fig. 12. Predicted temperature variation with depth at different heights within PV/PCM system type I at 80, 100 and 118 min.

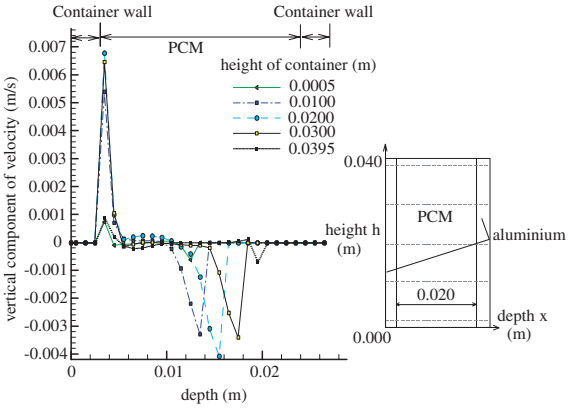

Fig. 13. The predicted vertical component of velocity with the depth at different heights within the PCM container at 80 min (system type I) with insolation of 1000 $W m^{-2}$ and ambient temperature of 20 °C.

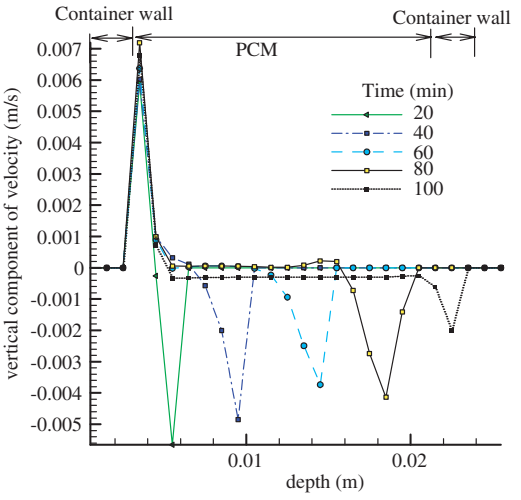

Fig. 14. The predicted vertical component of velocity with the depth at different times (system type I).

same as the predicted down flow at each height within the PCM within an error bound of ±0.02%. Fig. 14 shows a comparison of the vertical velocity component of the PCM at the middle height within PV/PCM system type I for five different times (corresponding to the predicted isotherms and velocity vectors for system type I shown in Fig. 11). As time progresses, the melt front extends further into PV/PCM system type I. The peak negative velocity in the vertical component remains adjacent to the melt front within the PCM. The downward vertical component of velocity decreases as time progresses, except at 80 min when it increased slightly due to the melt front reaching the back metal plate at this time. Cooled by the high thermal conductivity of the rear aluminium plate, the density of the molten PCM adjacent to the rear plate of the PCM container increases, leading to increased fluid flow in the PCM. The heat loss from the rear plate of the container also increases at this time. This reduced the temperature rise in the PCM. After 118 min the bulk flow in the fully molten PCM middle of the container exhibits a low downward

flow velocity. These results are consistent with the velocity vectors presented in Fig. 11.

5.3. Thermal control achieved for different ambient temperatures and insolations

The effect of ambient temperature on the temperature of the front surface of PV/PCM system type I is shown in Fig. 15. The ambient temperature was set to 10, 15 and 20 °C respectively. It can be seen that the predicted temperatures on the front surface of PV/PCM system type I are of a consistent form. By increasing the ambient temperature the temperature of the front surface does not change significantly, however as less heat is lost from the system, the time required for the PCM melting is reduced.

In order to evaluate the effect of incident insolation on the thermal behaviour of the system, simulations with incident insolation intensities of 600, 800 and 1000 $W\,m^{-2}$ were undertaken on system type I. The predicted temperature at the front surface of PV/PCM system type I for the three different levels of insolation are presented in Fig. 16. With increasing incident insolation intensity the temperature at the front surface increases and the melt time is reduced. Melting is complete 30 min sooner for a PV/PCM system type I exposed continually to 1000 $W\,m^{-2}$ when compared to continual exposure to 800 $W\,m^{-2}$.

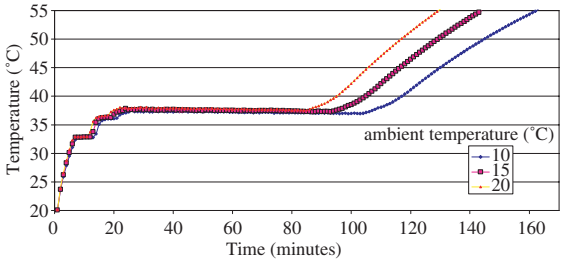

Fig. 15. Average temperature evolution at the front surface of system I with ambient temperatures set at 10, 15 and 20 °C with an insolation of 1000 $W\,m^{-2}$, and an initial system temperature of 20 °C.

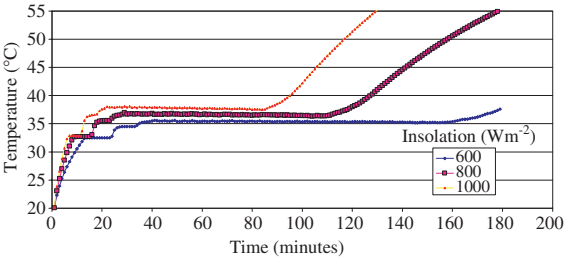

Fig. 16. Average predicted front surface temperatures with different levels of insolation for system I and an ambient temperature of 20 °C.

5.4. The effect of geometrical parameters of the PV/PCM system and fin design on thermal behaviour

To compare the moderating effect on the temperature of the PV/PCM system with varying geometries for the PV/PCM system, simulations for system types I, II and III with heights of 40, 132 and 132 mm were undertaken. The predicted average temperatures at system front surfaces are presented in Fig. 17. The temperatures increase rapidly for 6 min, the temperatures on the front surface of PV/PCM system type I then remain essentially constant through the PCM transition and then increased rapidly at phase change completion. After complete melting, because the product ρC_P for the liquid PCM is larger than that for the solid PCM the rate of temperature increase is slightly less than that during the solid stage. Comparing system I, with PCM height of 40 mm, to system type II, with PCM height of 132 mm, the average PV cell temperature (the temperature at the aluminium front surface of the system) increases, due to the increased size of the liquid PCM circulation. For system type III, which includes two fins, the temperature of the PV was maintained at 36.4 °C for 80 min. It is clear that aluminium fins enhance heat transfer into the PCM. For a single flat aluminium plate without PCM

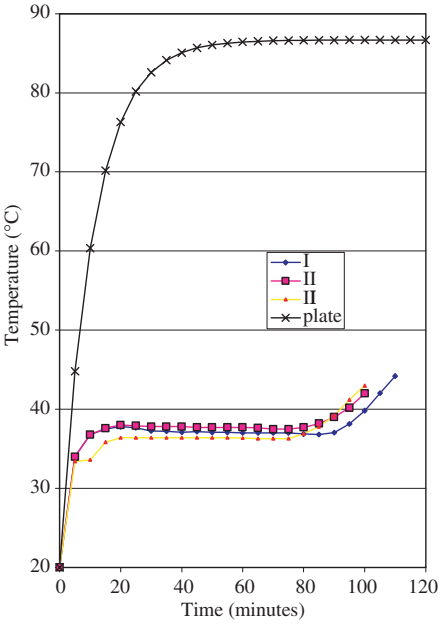

Fig. 17. Predicted average temperatures on the front surfaces of PV/PCM system types I, II and III when exposed to insolation of 1000 $W\,m^{-2}$ and an ambient temperature of 20 °C.

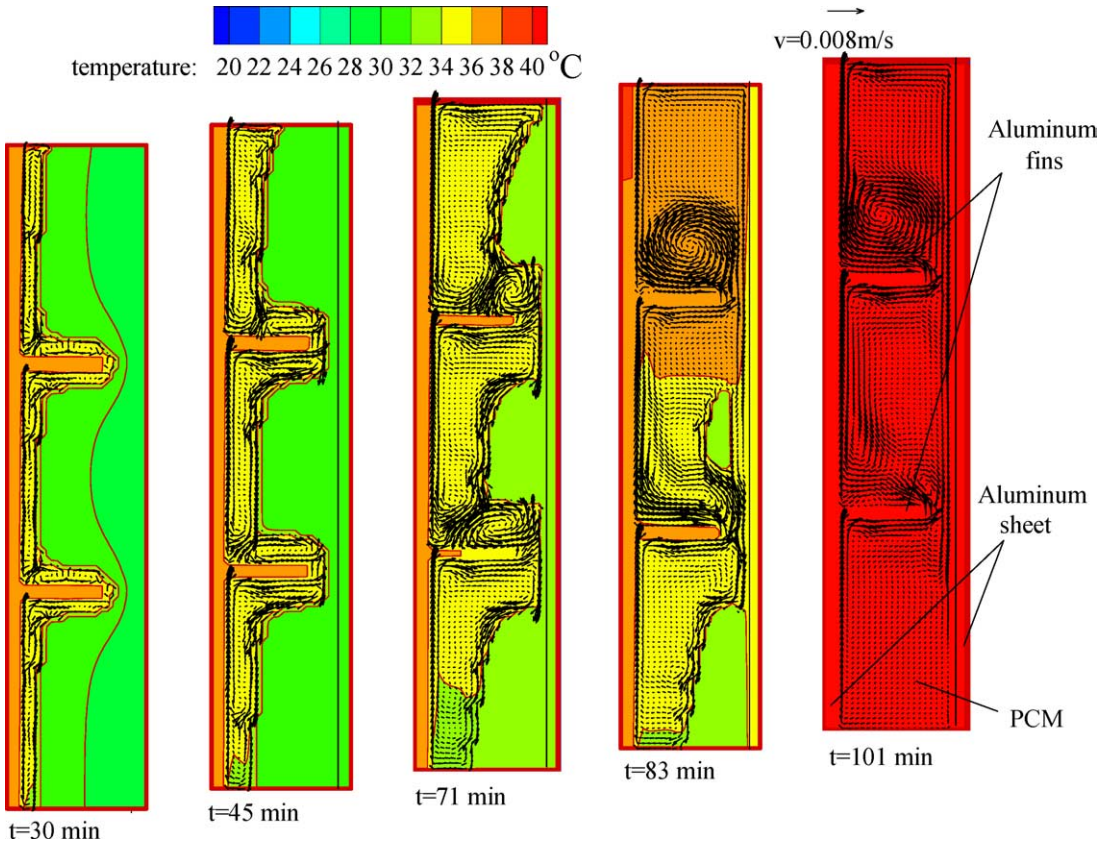

Fig. 18. Predicted isotherms and velocity vector diagrams for system III at different times.

(Fig. 17), the predicted temperature of the plate rises to 86.6 °C for the same boundary conditions. The potential benefits of using a finned PV/PCM system to moderate the PV temperature rise can be seen to be significant.

Predicted isotherms and velocity vector diagrams during the PCM melt process in PV/PCM system type III are shown in Fig. 18. After 45 min, a convective flow of hot molten PCM passes through the gap at the end of the fins into upper sections. Cooler molten PCM flows downward through the gap into lower sections. After 71 min, the molten PCM is in contact with the rear plate and the temperature of the rear plate increases above that of the solid PCM. This flow pattern is maintained until the PCM is fully molten. Once the PCM in the upper most section is fully molten at 83 min, the temperature at the front surface of PV/PCM system type III increases rapidly. The average temperature evolution in PV/PCM system type III with fins of thickness of 2, 3 and 4 mm is shown in Fig. 19. The variation of fin width is shown to be a marginal factor in improving performance.

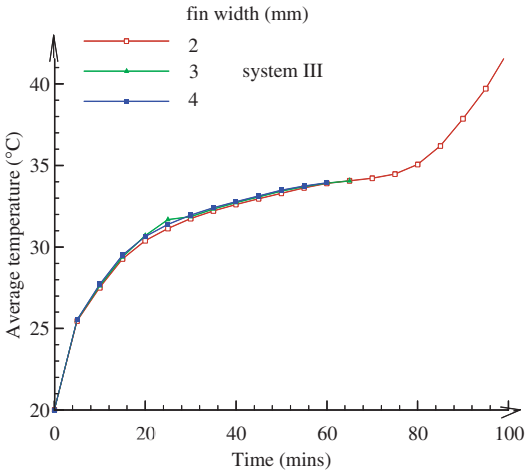

Fig. 19. Predicted average temperature evolution for system type III with different fin thickness with insolation of 1000 W m^{-2} and an ambient temperature of 20 °C.

Fig. 20 presents the PV temperature distribution on the surface of the PV/PCM system with different numbers of fins at a time of 70 min. The use of more thin fins provides improved thermal control. Increasing the

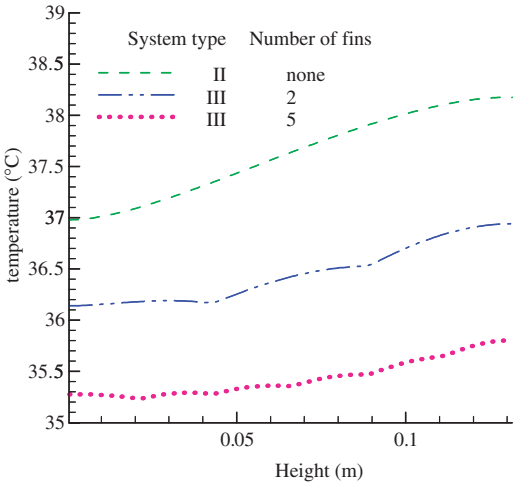

Fig. 20. Predicted front surface temperature variation with height within PV/PCM system without fins, with two and five fins after 70 min with insolation of 1000 W m^{-2} and an ambient temperature of 20 °C.

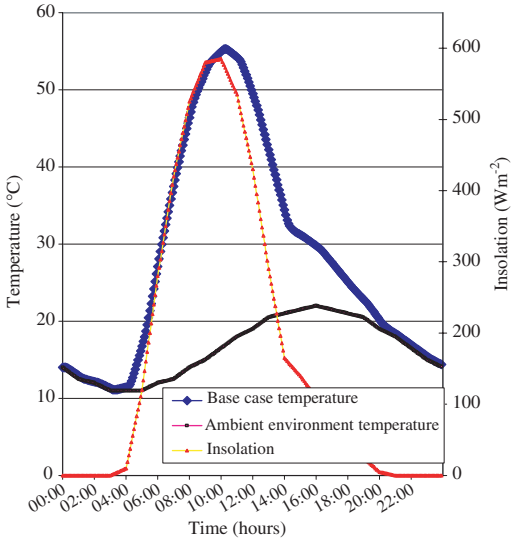

Fig. 21. 24 h predicted average temperature for the base case system in the south–east orientation in SE England with real insolation and ambient temperature on the 21st June.

number of fins to five can decrease the temperature difference on the front surface with height from 9.09 to 3.94 °C m^{-1} and also reduce the PV temperature.

5.5. Simulation under realistic ambient temperatures and insolation

The thermal control performance of a vertical south–east oriented PV/PCM system type I was predicted using realistic ambient temperature and insolation conditions for SE England for 21st June [42]. To predict long term temperature control, three days were simulated using weather data for the 21st June. For the simulation insolation and ambient temperatures were regarded as invariant over 5 min intervals. The initial system temperature was set to 14 °C at 00:00 h, the same as the ambient temperature.

The predicted temperature of a convectively cooled aluminium plate is shown in Fig. 21 together with the diurnal variation of insolation and ambient temperature. It can be seen that the temperature responds rapidly to the insolation intensity. When no insolation was incident the temperature of the base case aluminium plate returned rapidly to ambient.

The predicted diurnal temperatures at the front surface of PV/PCM system type I with 20 and 30 mm PCM depths and those for the base case aluminium plate are presented in Fig. 22. The temperatures at the front surface of PV/PCM system type I are maintained at a low temperature for a longer period than that for the base case aluminium plate. During phase change, the temperature at the front surface of PV/PCM system type I with 20 mm PCM is maintained below 35 °C, once the PCM became wholly liquid, the temperature of the PCM system rose rapidly. At 12:30 h the temperature at the front surface of the PV/PCM system reached a maximum of 45 °C. System type I with 30 mm PCM depth can maintain PV temperatures below 35 °C for the full 24 h period. It can be seen in Fig. 22 due to the low thermal conductivity of the PCM and energy stored, after 24 h the temperatures on the front surface of system I) with PCM depths of 20 and 30 mm were higher than their initial temperatures. A three day simulation using the weather data for the 21st of June was undertaken to predict the heat accumulation in the PV/PCM system with PCM depths of 20, 30 and 50 mm and is presented in Fig. 23. The predicted temperatures for the second and third day for all systems are essentially the same, the PCM has thus released all its latent heat to the ambient environment at night and returned to its solid phase at the start of each period of insolation. For the 50 mm depth of PCM a full transition to the molten state was not achieved, for this system design and conditions little is to be gained by increasing the depth of PCM beyond 30 mm.

The predicted PV electrical conversion efficiencies for an aluminium plate and system type I with PCM depths of 20 and 30 mm are compared in Fig. 24. A south–east orientation with insolation and ambient temperatures for the SE of England on 21st June for periods when the insolation was greater than 120 W m^{-2} are considered. For PV/PCM system with a PCM depth of 30 mm, PV electrical conversion efficiencies of over 15% were maintained at all times.

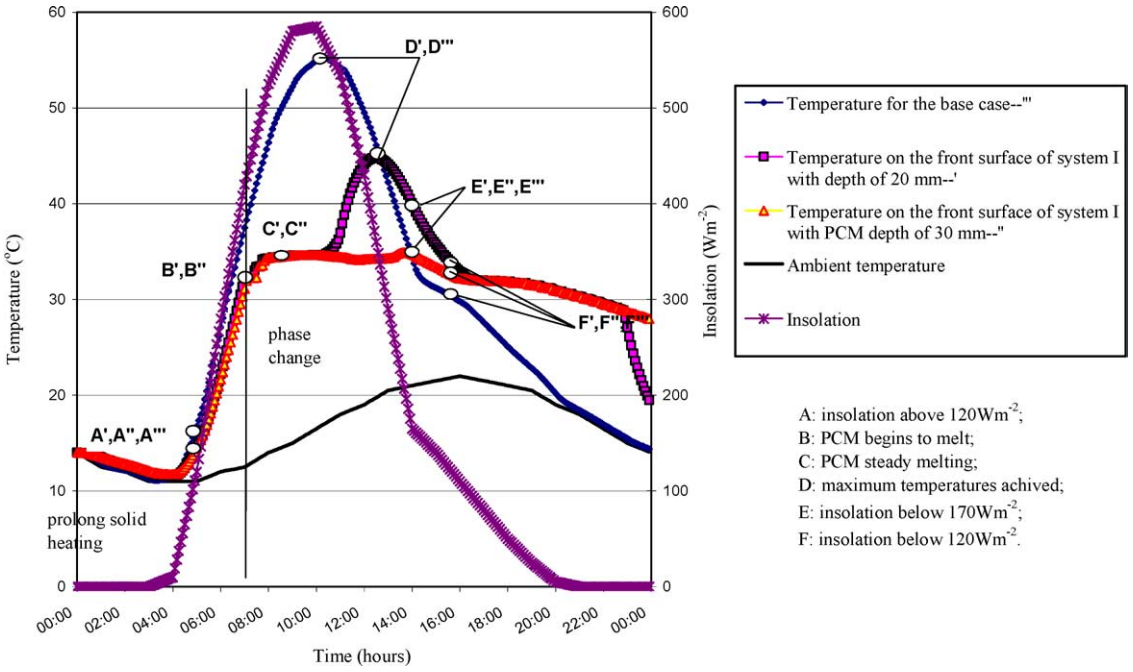

Fig. 22. 24 h predicted average temperatures on the front surface of the base case aluminium plate and at the front surface of system I with a PCM depth of 20 and 30 mm and south–east orientation with insolation and ambient temperature for SE England on the 21st June.

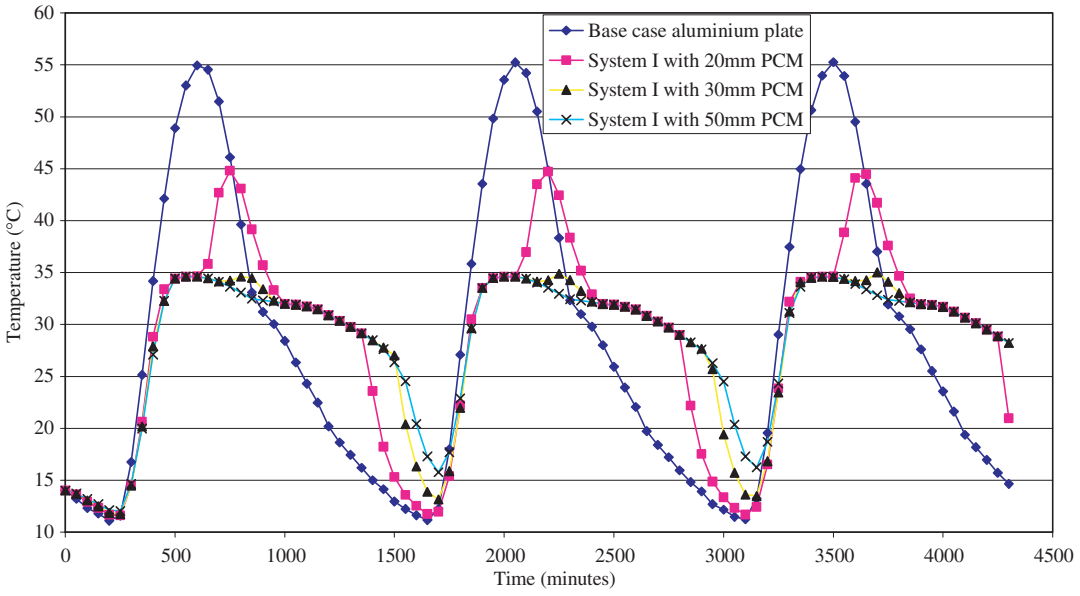

Fig. 23. Average temperature evolution for a three day simulation using the weather data for the 21st of June for the base case aluminium plate and at the front surface of PV/PCM system I with PCM depths of 20, 30 and 50 mm.

5.6. Non-temporal performance characterisation

If the difference in the specific heat of PCM in liquid and solid states is negligible, a heat balance on the PV/PCM system for unit surface area (assuming an initial temperature of T_{amb}) gives

$$\tau\alpha I_T \Delta t = \eta_c I_T \Delta t + U_L (T_{PV} - T_{amb}) \Delta t + Q_S \quad (10)$$

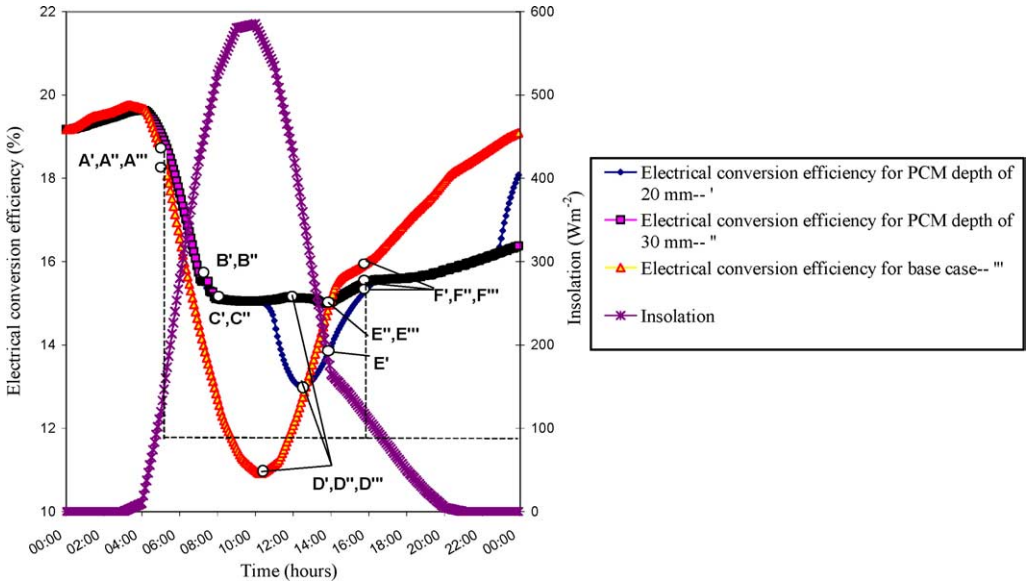

Fig. 24. 24 h predicted electrical conversion efficiency on the front surface of the base case aluminium plate and at the front surface of system type I with a PCM depth of 20 and 30 mm for a south–east orientation with insolation and ambient temperature for SE England on the 21st of June.

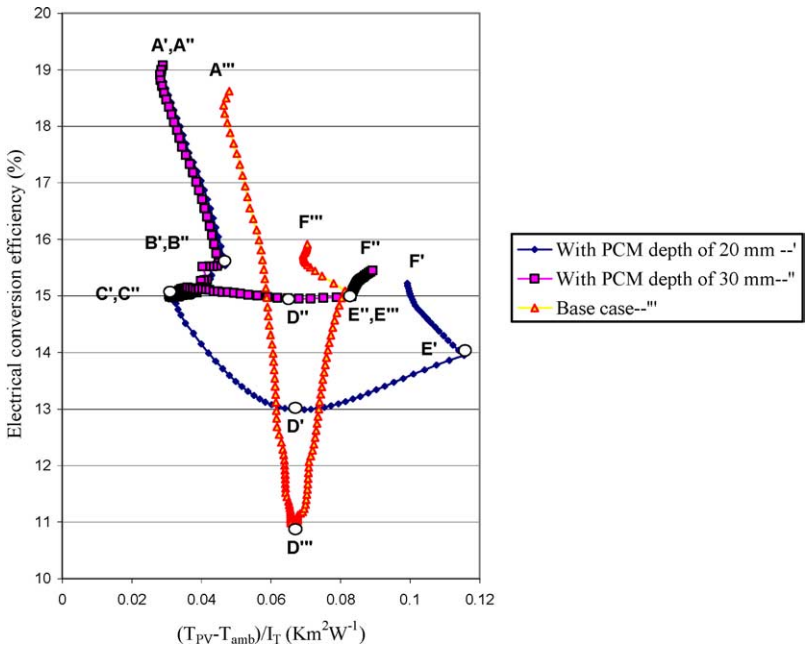

Fig. 25. 24 h predicted electrical conversion efficiency on the front surface of the base case aluminium plate and at the front surfaces of system I with a PCM depth of 20 and 30 mm with $(T_{PV} - T_{amb})/I_T$ for a south–east orientation with insolation and ambient temperature for SE England on the 21st of June. * T_{PV} and T_{amb} are the front surface temperature and ambient temperature, I_T is insolation $W\,m^{-2}$. Points A–F corresponds to those of Fig. 22.

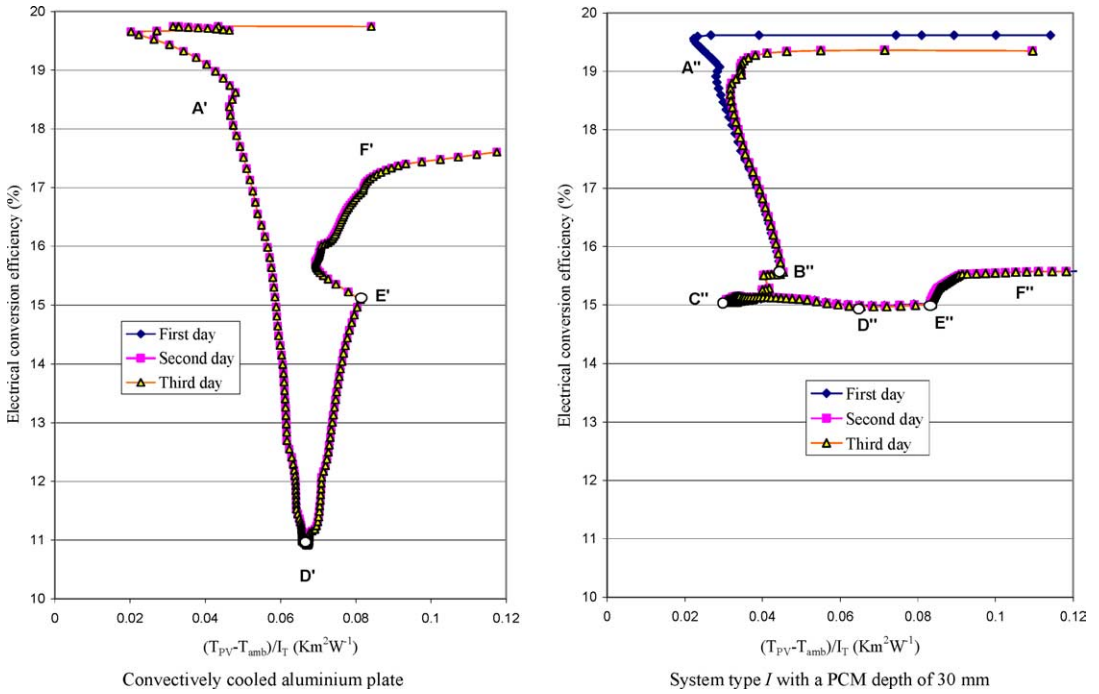

Fig. 26. A three day simulation using the weather data for the 21st June for electrical conversion efficiency on the front surface of the base case aluminium plate at the front surfaces of system I with a PCM depth of 30 mm with $(T_{PV} - T_{amb})/I_T$ for a south–east orientation with insolation and ambient temperatures for SE England.

The energy stored in the system is

$$Q_S = H + mc(T_{PV} - T_{amb}) \tag{11}$$

The PV electrical conversion efficiency is combining Eqs. (7) and (8) and rearranging:

$$\eta_c = \tau\alpha - U_L(T_{PV} - T_{amb})/I_T - (H + mc_P(T_{PV} - T_{amb}))/(I_T \Delta t) \tag{12}$$

so

$$\eta_c = (\tau\alpha - H/(\Delta t I_T)) - (U_L + mc_P/\Delta t)(T_{PV} - T_{amb})/I_T \tag{13}$$

A plot of η_c against $(T_{PV} - T_{amb})/(I_T \Delta t)$ enables a comparison of different PV/PCM systems to be made in terms of design conditions (i.e., insolation, ambient temperature) rather than behaviour with time. The electrical conversion efficiency against $(T_{PV} - T_{amb})/I_T$ shown in Figs. 25 and 26 give a comparison for the systems with realistic test conditions. The electrical conversion efficiency for the base case aluminium plate has the sharpest change in the narrowest range of $(T_{PV} - T_{amb})/I_T$ when compared to system I using PCM depths of 20 and 30 mm. The electrical efficiency for the system type I with 30 mm PCM depth was above 15% as shown in Fig. 25 even during the period of maximum insolation. Fig. 26 indicates electrical conversion efficiency with $(T_{PV} - T_{amb})/I_T$ for a three day simulation using weather for the 21st June for an aluminium plate and PV/PCM system type I with 30 mm PCM depth. The effect of PCM on the thermal performance for PV/PCM system is slightly different for the first day compared to the other two days. Graphs of the form of Fig. 26 can be employed to indicate long-term performance for different photovoltaic thermal management strategies for real insolation and ambient environment conditions.

6. Conclusion

The developed numerical PV/PCM model was validated successfully by comparison with experiments. This is to date the only numerical model for a system using PCM to moderate the temperature rise of PV that has been validated for identically sized geometries with realistic experimental conditions. The validated model provides a detailed insight into the thermal performance of a solid–liquid transition PCM when employed in a PV temperature control application.

At 1000 W m^{-2} insolation and an ambient temperature of 20 °C, for system type III (with two fins) with a PCM with a melt temperature of 32 °C and PCM depth of 20 mm the temperature on the front surface was

maintained at under 36.4 °C for 80 min. For a PCM with a melt temperature of 26.6 °C, a PCM depth of 40 mm, at 750 $W m^{-2}$ insolation and 20 °C ambient temperature the temperature at the front surface of system type III was maintained at under 33 °C for 150 min. The predicted thermal control performance for a vertical south–east oriented PV/PCM system type I using realistic ambient temperature and insolation conditions in SE England for 21st June has been presented. A PCM depth of 30 mm within PV/PCM system type I can maintain the temperature on the front surface of the system, at under 35 °C using repeated UK weather data for the 21st of June for three days. From the predictions for the three day simulation it can be seen, that for a PCM depth of 30 mm, the highest temperatures attained was 34 °C, about two degrees higher than the transition temperature. To maintain the temperature on the front surface of the PV/PCM system at 25 °C, the characterising temperature of the PV, the set transition temperature of the PCM should be higher than the ambient temperature and lower than 25 °C. The improvement in the thermal performance achieved by using metal fins in the PCM container is significant. The fins enable a more uniform temperature distribution within the PV/PCM system to be maintained. Natural convective flows in the molten PCM increase the heat transfer within the PCM further improving the capacity of the thermal control effect on the PV. However increased numbers of fins can limit the movement of molten PCM. The relationship between the number and geometry of fins and the convective flow requires further study.

Acknowledgements

A University of Ulster Research Scholarship is hereby acknowledged. This research was supported by the Engineering and Physical Science Research Council, Swindon, UK. Thanks also to Mr. Frank Stewart for his assistance in the experimental work and the Schumann Company for providing phase change materials.

References

[1] J.G. Ingersoll, Simplified calculation of solar cell temperatures in terrestrial photovoltaic arrays, ASME J. Solar Energy Eng. 108 (1986) 95–101.
[2] S. Krauter, R. Hanitsch, S.R. Wenham, Simulation of thermal and optical performance of PV modules, Part III, Renew. Energy 5 (1994) 1701–1703.
[3] S. Krauter, R. Hanitsch, P. Campbell, S.R. Wenham, Simulation tool for prediction and optimization of output power considering thermal and optical parameters of PV module encapsulation, in: Proceedings of 12th European Photovoltaic Solar Energy Conference, Amsterdam, Holland, 1994, pp. 1194–1197.
[4] P. Batagiannis, C. Gibbons, Thermal assessment of silicon-based composite materials used in photovoltaics, in: Proceedings of Renewable Energy in Maritime Island Climates Conference, Belfast, September, UK, 2001, pp. 151–157.
[5] S. Sick, T. Erge (Eds.), Photovoltaics in Buildings: A Design Handbook for Architects and Engineers, James and James, London, 1996.
[6] D. Goossens, E.V. Kerschaever, Aeolian dust deposition on photovoltaic solar cells: the effects of wind velocity and airborne dust concentration on cell performance, Solar Energy 66 (1999) 277–289.
[7] E. Bilgen, Passive solar massive wall systems with fins attached on the heated wall and without glazing, ASME J. Solar Energy Eng. 122 (2000) 30–34.
[8] A. Abhat, Low temperature latent heat thermal energy storage: heat storage materials, Solar Energy 30 (1983) 313–332.
[9] J.A. Duffie, W.A. Beckman, Solar Engineering of Thermal Processes, Wiley & Sons, USA, 1991.
[10] K. Ismail, M. Goncalves, Thermal performance of a PCM storage unit, Energy Convers. Manage. 40 (1999) 115–138.
[11] R.A. Wirtz, N. Zheng, D. Chandra, Thermal management using "dry" phase change materials, in: Proceedings of Fifteen IEEE Semiconductor Thermal Measurement and Management Symposium, March 9–11, San Diego, CA, USA, IEEE#99CH36306, 1999, pp. 74–82.
[12] J. Paris, F. Villain, J.-F. Houle, Incorporation of PCM in wallboards: a review of recent developments, in: Proceedings of the 1st World Renewable Energy Congress, September, Reading, UK, 1990, pp. 2397–2401.
[13] M.M.D. Shapiro, D. Feldman, D. Hawes, D. Banu, PCM thermal storage in wallboard, in: Proceedings of 12th Passive Solar Conference, Portland, USA, 1987, pp. 38–58.
[14] K.A.R. Ismail, J.R. Henriquez, Thermally effective windows with moving phase change material curtains, Appl. Thermal Eng. 21 (2001) 1909–1923.
[15] M. Esen, Thermal performance of a solar-aided latent heat store used for space heating by heat pump, Solar Energy 69 (2000) 15–25.
[16] O. Comakli, K. Kaygusuz, T. Ayhan, Solar-assisted heat pump and energy storage for residential heating, Solar Energy 51 (1993) 357.
[17] I. Dincer, M.A. Rosen, Thermal Energy Storage, John Wiley & Sons, England, 2002, pp. 303–335.
[18] V.R. Voller, An overview of numerical methods for solving phase change problems, in: W.J. Minkowycz, E.M. Sparrow (Eds.), Advances in Numerical Heat Transfer, Taylor & Francis, New York, 1997, pp. 341–380 (Chapter 9).
[19] J. Fukai, Y. Hamada, Y. Morozumi, O. Miyatake, Improvement of thermal characteristics of latent heat thermal energy storage units using carbon-fibre brushes: experiments and modelling, Int. J. Heat Mass Transfer 46 (2003) 4513–4525.
[20] P. Brousseau, M. Lacroix, Numerical simulation of a multi-layer latent heat thermal energy storage system, Int. J. Energy Res. 22 (1998) 1–15.
[21] M. Lacroix, Numerical simulation of a shell-and-tube latent heat thermal energy storage unit, Solar Energy 50 (4) (1993) 357–367.
[22] M. Lacroix, Study of the heat transfer behaviour of a latent heat thermal energy storage unit with a finned tube, Int. J. Heat Mass Transfer 36 (8) (1993) 2083–2092.

[23] M. Farid, R. Husian, An electrical storage heater using the phase-change method of heat storage, Energy Convers. Manage. 30 (3) (1990) 219–230.
[24] O. Bertrand, B. Binet, H. Combeau, S. Couturier, Y. Delannoy, D. Gobin, M. Lacroix, P. Le Quere, M. Medale, J. Mencinger, H. Sadat, G. Vieira, Melting driven by natural convection: a comparison exercise, Int. J. Thermal Sci. 38 (1999) 5–26.
[25] B. Binet, M. Lacroix, Numerical study of natural-convection dominated melting inside uniformly and discretely heated rectangular cavities, J. Numer. Heat Transfer—Part A 33 (1998) 207–224.
[26] M. Lacroix, M. Benmadda, Numerical simulation of natural convection dominated melting and solidification from a finned vertical wall, Numer. Heat Transfer—Part A 31 (1997) 71–86.
[27] M. Lacroix, M. Benmadda, Analysis of natural convection melting from a heated wall with vertically oriented fins, Int. J. Numer. Methods Heat Fluid Flow 8 (4) (1998) 465–478.
[28] A. Sasaguchi, K. Kusano, R. Viskanta, A numerical analysis of solid–liquid phase change heat transfer around a single and two horizontal, vertical spaced cylinders in a rectangular cavity, Int. J. Heat Mass Transfer 40 (6) (1997) 1343–1354.
[29] Y.K. Wu, M. Lacroix, Analysis of natural convection melting of a vertical ice cylinder involving density anomaly, Int. J. Numer. Methods Heat Fluid Flow 3 (1993) 445–456.
[30] Y.K. Wu, M. Lacroix, Melting of a PCM inside a vertical cylindrical capsule, Int. J. Numer. Methods Fluids 20 (1995) 559–572.
[31] M. Huang, P.C. Eames, B. Norton, An experimental study into the application of phase change materials to limit the temperature rise in build integrated photovoltaic systems, in: Proceedings of Renewable Energy in Maritime Island Climates, September, Belfast, UK, 2001, pp. 143–150.
[32] M. Huang, The application of CFD to predict the thermal performance of phase change materials for the control of photovoltaic cell temperature in buildings, Ph.D. Thesis, University of Ulster, UK, 2002.
[33] M. Huang, P.C. Eames, B. Norton, The application of computational fluid dynamics to predict the performance of phase change materials for control of photovoltaic cell temperature in buildings, in: Proceedings of VI World Renewable Energy Congress, July, Brighton, UK, 2000, pp. 2123–2126.
[34] S.V. Patankar, Numerical Heat Transfer and Fluid Flow, Hemisphere Publishing Corporation, London, 1980.
[35] M. Huang, P.C. Eames, B. Norton, Experimental validation of a numerical model for the prediction of thermal regulation of building-integrate photovoltaics using phase change materials, in: Proceedings of VII World Renewable Energy Congress, July, Cologne, Germany, 2002, pp. 2123–2126.
[36] Anon (a), MAXORB data sheet, RS Components Ltd., UK, 2000.
[37] Anon (b), RUBITHERM data sheet, Co. RUBITHERM GmbH, Hamburg, Germany, 2000.
[38] D.V. Hale, M.J. Hoover, M.J. O'Neil, Phase Change Materials Handbook, NASA CR 61363, 1975.
[39] W.M. Rohsenow, J.P. Hartnett, Y.I. Cho, Handbook of Heat Transfer, third ed., McGraw-Hill, New York, 1998.
[40] Anon (c), Kipp & Zonen data sheet, Kipp & Zonen Ltd., UK, 2000.
[41] Y. Bayazitoglu, M.N. Ozisik, Elements of Heat Transfer, McGraw-Hill book company, London, 1998.
[42] CIBSE, Student Members Data Book, second ed., Chartered Institute of Building Services Engineers, London, UK, 1991.